SLS Integrated Modal Test Uncertainty Quantification using the Hybrid Parametric Variation Method

Daniel C. Kammer, Paul Blelloch[1], and Joel Sills[2]

[1]ATA Engineering, Inc
13290 Evening Creek Drive S, San Diego, CA 92128

[2]NASA Johnson Space Center
2101 E. NASA Parkway, Houston, TX 77058

ABSTRACT

Uncertainty in structural loading during launch is a significant concern in the development of spacecraft and launch vehicles. Small variations in launch vehicle and payload mode shapes and their interaction can result in significant variation in system loads. In many cases involving large aerospace systems it is difficult, not economical, or impossible to perform a system modal test. However, it is still vital to obtain test results that can be compared with analytical predictions to validate models. Instead, the "Building Block Approach" is used in which system components are tested individually. Component models are correlated and updated to agree as best they can with test results. The Space Launch System consists of a number of components that are assembled into a launch vehicle. Finite element models of the components are developed, reduced to Hurty/Craig-Bampton models and assembled to represent different phases of flight. The only opportunity to obtain modal test data from an assembled Space Launch System will be during the Integrated Modal Test. There is always uncertainty in every model, which flows into uncertainty in predicted system results. Uncertainty Quantification is used to determine statistical bounds on prediction accuracy based on model uncertainty. For the Space Launch System, model uncertainty is at the Hurty/Craig-Bampton component level. Uncertainty in the Hurty/Craig-Bampton components is quantified using the hybrid parametric variation approach that combines parametric and nonparametric uncertainty. Uncertainty in model form is one of the biggest contributors to uncertainty in complex built-up structures. This type of uncertainty cannot be represented by variations in finite element model input parameters and thus cannot be included in a parametric approach. However, model-form uncertainty can be modeled using a nonparametric approach based on random matrix theory. The hybrid parametric variation method requires the selection of dispersion values for the Hurty/Craig-Bampton fixed-interface eigenvalues, and the Hurty/Craig-Bampton stiffness matrices. Component test/analysis frequency error is used to identify the fixed-interface eigenvalue dispersions, while test/analysis cross-orthogonality is used to identify stiffness dispersion values. The hybrid parametric variation uncertainty quantification approach is applied to the Space Launch System Integrated Modal Test configuration. Monte Carlo analysis is performed, and statistics are determined for modal correlation metrics, frequency response from Integrated Modal Test shakers to selected accelerometers, as well as other metrics for determining how well target modes are excited and identified. If the predicted uncertainty envelopes future Integrated Modal Test results, then there will be increased confidence in the utility of the component-based hybrid parametric variation uncertainty quantification approach.

Keywords: Uncertainty Quantification, Hurty/Craig-Bampton, Random Matrix, Model Form

ACRONYMS

CAA	Crew Access Arm
CL	Centerline

CS	Core Stage
CT	Crawler Transporter
DCGM	Diagonal Cross-Generalized Mass
DOF	Degree of Freedom
FEM	Finite Element Model
FI	Fixed Interface
GP	Gaussian Process
HCB	Hurty/Craig-Bampton
HPV	Hybrid Parametric Variation
ICPS	Interim Cryogenic Propulsion Stage
ISPE	Integrated Spacecraft Payload Element
IVGVT	Integrated Vehicle Ground Vibration Test
IMT	Integrated Modal Test
LSRB	Left Solid Rocket Booster
LV	Launch Vehicle
LVSA	Launch Vehicle Stage Adapter
MC	Monte Carlo
MEM	Modal Effective Mass
ML	Mobile Launcher
MPCV	Multipurpose Crew Vehicle
MSA	MPCV Stage Adapter
MSO	Mass Simulator for Orion
NMIF	Normal Mode Indicator Function
NPV	Nonparametric Variation
RMS	Root Mean Square
RMT	Random Matrix Theory
RSRB	Right Solid Rocket Booster
RSS	Root Sum Square
RV	Residual Vector
SLS	Space Launch System
SRB	Solid Rocket Booster (Solid Rocket Motor)
TAM	Test Analysis Model
UQ	Uncertainty Quantification
VAB	Vertical Assembly Building
XO	Cross-Orthogonality

INTRODUCTION

NASA has historically tested launch vehicles in an integrated configuration with boundary conditions controlled to approximate the boundary conditions expected in flight. Integrated Vehicle Ground Vibration Tests (IVGVT) increase confidence that structural loads predicted using system finite element models are within specified limits with respect to accuracy and uncertainty. However, to save cost and schedule, a cross-program decision was made to not perform the IVGVT for the Space Launch System (SLS) and rely more heavily on analytical methods supported by component test results. This process is referred to as the “building-block approach”, in which system components are tested individually, and component models are correlated and updated to agree with test results as closely as possible.

In spite of this decision, an integrated SLS system will still undergo testing, referred to as the Integrated Modal Test (IMT). The IMT is a ground test of the integrated vehicle, assembled on the Mobile Launcher (ML) in the Vehicle Assembly Building (VAB) facility at Kennedy Spaceflight Center. The results of the IMT will provide an opportunity to validate or update previously correlated SLS component models such that, in an assembled configuration, they provide agreement with integrated system test results. For this test, the integrated SLS is mounted to the launch pad at the base of the solid rocket boosters with the Multi-Purpose Crew Vehicle (MPCV) replaced by the Mass Simulator for Orion (MSO). The IMT/MSO configuration, shown in Figure 1, is resting on the 6 VAB support posts with no Crawler Transporter (CT). The analytical model used in this study consists of SLS Hurty/Craig-Bampton (HCB) components developed based on the IMT integrated FEM. The Interim Cryogenic Propulsion Stage (ICPS) and core stage (CS) are empty, with CS pressurization stiffness

included corresponding to approximately four psi. The integrated model was divided into six HCB [1] components including the MSO combined with the MPCV Spacecraft Adaptor (MSA), a combined ICPS and Launch Vehicle Stage Adapter (LVSA), the CS, left and right Solid Rocket Boosters (LSRB, RSRB), and the ML.

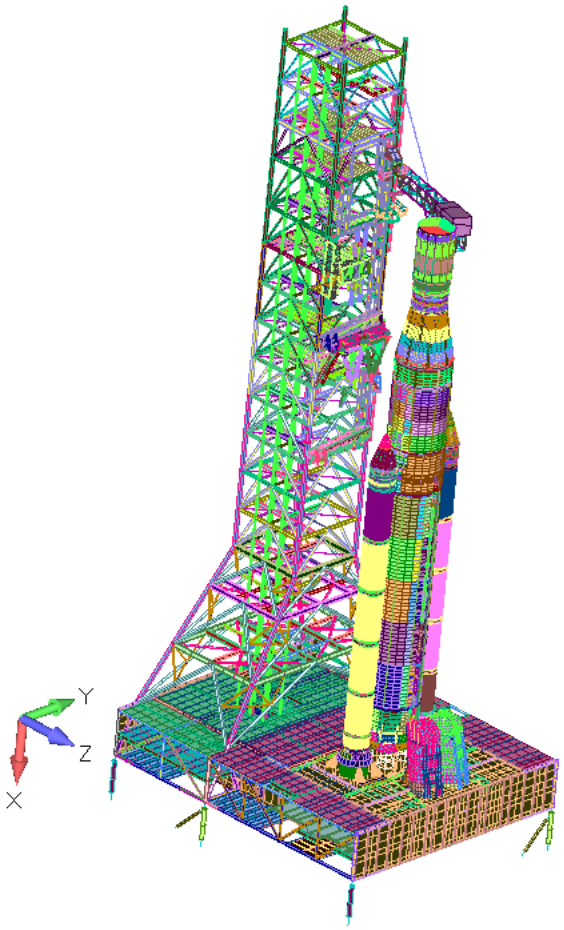

Figure 1: IMT with MSO on six VAB mounts

There is some level of uncertainty in every analytical model, which flows to a level of uncertainty in predicted results. The purpose of uncertainty quantification (UQ) is to provide statistical bounds on prediction accuracy based on model uncertainty. This is distinct from model updating, which attempts to modify models to improve their accuracy. Uncertainty quantification does not improve the accuracy of models, but accepts the fact that the models are inaccurate and attempts to quantify the impact of that inaccuracy on predicted results. Previously, a new method for UQ, called the Hybrid Parametric Variation (HPV) method, was applied to SLS HCB components to predict system level statistics for SLS attitude control transfer functions [2] and CS section loads due to buffet [3]. The HPV method combines a parametric variation of the HCB fixed-interface (FI) modal frequencies with a nonparametric variation (NPV) method that randomly varies the HCB mass and stiffness matrices as Wishart [4] random matrix distributions using random matrix theory (RMT). The HPV method anchors uncertainty at the HCB level to component modal test results by matching HCB modes to test configuration modes based on either modal effective mass (MEM) or mode descriptions, and then applying differing levels of frequency variation. The specific variations depend on the degree to which a component FEM has been verified through modal testing. The NPV method is then layered on top of the frequency variation, to match modal test cross-orthogonality (XO) results. The component uncertainty is propagated to the system level using a Monte Carlo (MC) approach that generates statistics for system-level results. This provides a UQ method that can be traced directly to available test data, and which can be updated as additional data and better correlated models become available.

The purpose of this study was to apply the HPV UQ approach to the IMT/MSO ground vibration test. Projection of component test-based uncertainty into the system provides estimates of the system level uncertainty that can be expected in target modal parameters, such as frequencies and mode shapes. Component uncertainty is also propagated into system level frequency response and normal mode indicator functions (NMIF) [5]. Statistics for NMIF and modal orthogonality can be used during pretest analysis to determine the probability that the target modes will be adequately excited and separated during the modal test using the proposed sensor and shaker configurations. This study was completed prior to the IMT, however, during future post-test analysis, the test results can be compared to the UQ predictions. If the uncertainty predicted by the UQ analysis covers the test results, there is increased confidence that the HPV UQ method and the approach used to assign component uncertainty models are valid. This paper presents a brief summary of the theory behind the NPV and HPV methods including new developments, a description of the IMT components and corresponding component uncertainty models, followed by the presentation of MC based statistics for target modal parameters, selected frequency response functions, and normal mode indicator functions. At the time of this study, model correlation and updating of the ML was still in progress, meaning that the sensor set and shaker locations were still evolving. It has been found that the ability of the shaker configuration to adequately excite the target modes is very much dependent on the most recent updated ML model version. Therefore, some of the statistics presented in this report must be considered as preliminary.

THEORY

The SLS consists of components that are assembled into the launch vehicle. In order to predict system performance, FEMs of the components are developed, reduced to HCB representations, and assembled to represent different phases of flight. The same approach is used for IMT. There is always uncertainty in every model, which flows into uncertainty in predicted system results. For the SLS, it is natural to treat the model uncertainty at the HCB component-model level. The HCB component-model displacement vector is given by $u_{HCB} = \{x_t^T \quad q^T\}^T$, where x_t is the vector of physical displacements at the component interface and q is the vector of generalized coordinates associated with the component fixed-interface (FI) modes. Given the assumption that the FI modes are mass normalized, the corresponding HCB mass and stiffness matrices have the form

$$M_{HCB} = \begin{bmatrix} M_S & M_{tq} \\ M_{tq}^T & I \end{bmatrix} \qquad K_{HCB} = \begin{bmatrix} K_S & 0 \\ 0 & \lambda \end{bmatrix} \tag{1}$$

in which M_S and K_S are the component physical mass and stiffness matrices statically reduced to the interface, M_{tq} is the mass coupling between the interface and the fixed-interface modes, I is an identity matrix, and λ is a diagonal matrix of the FI mode eigenvalues. Details of the HCB component-model derivation can be found in reference [1].

In this work, uncertainty in the component HCB representations is quantified using the HPV approach, which combines parametric with nonparametric uncertainty. Purely parametric uncertainty approaches are the most common in the structural dynamics community. Component parameters that are inputs to the FEM, such as Young's modulus, mass density, geometric properties, etc., are modeled as random variables. Parametric uncertainty can be propagated into the system response using a method such as stochastic finite element analysis [6]. The advantage of the parametric approach is that each random set of model parameters represents a specific random FEM. However, there are disadvantages associated with the parametric method: it can be very time consuming, there are an infinite number of ways to parameterize the model, and the selected parameter probability distributions are generally not available. The most significant drawback is that the uncertainty represented is limited to the form of the nominal FEM. It is known that most errors in a FEM stem from modeling assumptions or model-form errors, not parametric errors. Therefore, in practice, the parameter changes are merely surrogates for the actual model errors. In the case of HPV, the HCB components are parameterized in terms of the FI eigenvalues, not the inputs to the original FEM. While there is not a simple direct connection between the random FI eigenvalues and a random component FEM, there is a direct connection to the corresponding random HCB component.

Model-form is likely the largest contributor to uncertainty in complex built-up structures, as it cannot be directly represented by model parameters and thus cannot be included in a parametric approach. Familiar examples include unmodeled nonlinearities, errors in component joint models, etc. Instead, model-form uncertainty can be represented using RMT, where a probability distribution is developed for the matrix ensemble of interest. RMT was introduced and developed in mathematical statistics by Wishart [4], and more recently, Soize [7] [8] developed an NPV approach to represent model-form

uncertainty in structural dynamics applications. Soize's approach was extended by Adhikari [9] [10] using Wishart distributions to model random structural mass, damping, and stiffness matrices. The nonparametric matrix-based approach to representing structural uncertainty has been used previously in several aeronautics and aerospace engineering applications [11] [12] [13].

The maximum entropy (ME) principle was employed by Soize [8] to derive the positive and positive-semidefinite ensembles SE^{+} and SE^{+0} that follow a matrix variate gamma distribution and are capable of representing random structural matrices. This means that the matrices in the ensembles are real and symmetric and possess the appropriate sign definiteness to represent structural mass, stiffness, or damping matrices. As the dimension of the random matrix *n* increases, the matrix variate gamma distribution converges to a matrix variate Wishart distribution. The matrix dimensions in structural dynamics applications are usually sufficient to give a negligible difference between the two distributions. In letting ensemble member random matrix *G* be any of the random mass, stiffness, or damping matrices, it is assumed that *G* follows a matrix variate Wishart distribution, $G \sim W_n(p, \Sigma)$. A Wishart distribution with parameters *p* and Σ can be thought of as the sum of the outer product of *p* independent random vectors X_i all having a multivariate normal distribution with zero mean and covariance matrix Σ. Parameter *p* is sometimes called the shape parameter. The random matrix *G* can be written as

$$G = \sum_{i=1}^{p} X_i X_i^T \qquad X_i \sim N_n(0, \Sigma) \tag{2}$$

where the expected value is given by

$$E(G) = \bar{G} = p\Sigma \tag{3}$$

The dispersion or normalized standard deviation of the random matrix *G* is defined by the relation

$$\delta_G^2 = \frac{E\left(\|G - \bar{G}\|_F^2\right)}{E\left(\|\bar{G}\|_F^2\right)} \tag{4}$$

in which $\|*\|_F^2$ is the Frobenius norm squared, or $\text{trace}(*^T *)$. It can be shown that Eq. (4) reduces to the expression

$$\delta_G^2 = \frac{1}{p}\left[1 + \frac{\left(tr(\bar{G})\right)^2}{tr(\bar{G}^T\bar{G})}\right] = \frac{1}{p}[1 + \gamma_G] \tag{5}$$

where $\gamma_G = \frac{\left(tr(\bar{G})\right)^2}{tr(\bar{G}^T\bar{G})}$ can be thought of as a measure of the magnitude of the matrix. The uncertainty in the random matrix *G* is dictated by the shape parameter *p*, the number of inner products in Eq. (2). The larger the value of *p*, the smaller the dispersion δ_G. There may be instances when it is desirable to have the same amount of uncertainty in two or more substructures. Suppose G_1 and G_2 represent structural matrices, such as stiffness, from two different system components. In order to have equivalent uncertainty in the two matrices, the shape parameter *p* must be the same for both ensembles. However, Eq. (5) shows that even if $p_1 = p_2 = p$, the dispersion values are not the same in general, $\delta_{G_1}^2 \neq \delta_{G_2}^2$, unless $\gamma_1 = \gamma_2$. A more useful definition of matrix dispersion is the normalized dispersion

$$\delta_{G_n} = \frac{\delta_{G_1}}{\sqrt{1+\gamma_1}} = \frac{\delta_{G_2}}{\sqrt{1+\gamma_2}} = \frac{1}{\sqrt{p}} \tag{6}$$

which is independent of the matrix magnitude γ_G.

Adhikari [9] referred to the random matrix method developed by Soize [7] [8] as Method 1. The Wishart parameters are selected as p and $\Sigma = G_o/p$ where G_o is the nominal value of *G*. The mean of the distribution is given by Eq. (3) as $\bar{G} = p\Sigma = p(G_o/p) = G_o$. Therefore, Method 1 preserves the nominal matrix as the mean of the ensemble. In general, the nominal matrix can be decomposed in the form

$$G_o = LL^T \tag{7}$$

In the case of a positive definite matrix, this would just be the Cholesky decomposition. Let $(n \times p)$ matrix *X* be given by

$$X = \begin{bmatrix} x_1 & x_2 \cdots x_p \end{bmatrix} \tag{8}$$

in which x_i is an $(n \times 1)$ column vector containing standard random normal variables such that $x_i \sim N_n(0, I_n)$. Note that $p \geq n$ must be satisfied in order for G to be full rank. An ensemble member $G \sim W_n(p, G_o/p)$ can then be generated for MC analysis using the expression

$$G = \frac{1}{p} LXX^T L^T \tag{9}$$

It has been found that ensembles of random component mass matrices are best represented using Method 1. Adhikari [9] noted that Method 1 does not maintain the inverse of the mean matrix as the mean of the inverse; that is

$$E(G^{-1}) \neq [E(G)]^{-1} = \bar{G}^{-1} \tag{10}$$

The two can be vastly different in some cases, which is clearly not physically realistic. Instead, he proposed Method 3, in which the Wishart parameters are selected as p and $\Sigma = G_o/\theta$ where

$$\theta = \frac{1}{\delta_G^2}[1 + \gamma_G] - (n + 1) \tag{11}$$

An ensemble member $G \sim W_n(p, G_o/\theta)$ can then be generated using the relation

$$G = \frac{1}{\theta} LXX^T L^T \tag{12}$$

In this case, the inverse of the mean matrix is preserved as the mean of the ensemble inverses, where the mean matrix is now given by

$$\bar{G} = p\Sigma = p(G_o/\theta) = \frac{p}{\theta} G_o \tag{13}$$

In Method 3, the dispersion defined in Eq. (4) is now calculated with respect to the mean given in Eq. (13), while Eqs. (5) and (6) still hold. It has been determined that ensembles of random component stiffness matrices are best represented using Method 3. Therefore, the nonparametric portion of the HPV method is based on a Method 1 randomization of the component mass matrix and a Method 3 randomization of the component stiffness matrix. In IMT application, only the component stiffness matrices are randomized. The component mass matrices are assumed to have little uncertainty and are assumed to be deterministic.

The Wishart matrix uncertainty model results in uncertainty in both frequencies and mode shapes. However, an extensive amount of MC simulation and analysis performed during this and previous assessments has shown that, in comparison to modal frequencies, the corresponding component mode shapes tend to be much more sensitive to the nonparametric matrix randomization provided by Methods 1 and 3. Therefore, the HPV approach possesses a parametric component of uncertainty in which the eigenvalues of the FI modes in the component HCB representation are assumed to be random variables. The FI eigenvalues are then random parameters within the HCB component stiffness matrix. During each iteration within an MC analysis, a random draw of HCB FI eigenvalues is selected to generate a random HCB component stiffness matrix. Note that the mean of this ensemble would just be the nominal HCB stiffness matrix. However, for the current iteration, the parametrically randomized HCB stiffness is treated as the nominal matrix for NPV, and Method 3 is applied to provide model-form uncertainty on top of the FI eigenvalue uncertainty. This is analogous to the approach proposed by Capiez-Lernout [11] for separating parametric and nonparametric uncertainty. In contrast to the nonparametric model-form uncertainty, the mode shapes are relatively insensitive to the parametric FI eigenvalue uncertainty. Therefore, the HPV approach provides the capability to almost independently adjust the uncertainty in the component frequencies and mode shapes when the uncertainty levels are not too high.

The HPV method also has the capability of preserving rigid body motion and rigid body mass properties. It can also preserve the certainty of subsets of component modes. For example, in previous assessments, the component slosh modes were assumed to have no uncertainty. Details on how to handle these special cases are presented in reference [2].

Randomization of Component FI Eigenvalues using Gaussian Process Models

In past work [2] [3], the component FI eigenvalues were considered as independent random variables. It was shown in reference [3] that even though the variation of the FI eigenvalues is parametric with respect to the HCB representation, if they are varied independently, it results in nonparametric variation of the stiffness matrix in physical space. In contrast, if the FI eigenvalues are varied in unison, i.e. perfectly correlated, it produces a purely parametric variation of the component stiffness matrix in physical space. As a component stiffness matrix varies, it is common to see the corresponding eigenvalues vary in a correlated manner to some extent, especially when they are closely spaced. Therefore, reality is somewhere between treating the FI eigenvalues as totally independent and treating them as perfectly correlated.

In this study, Gaussian Process (GP) modeling [14] was used to represent the random space of component FI eigenvalues. This means that any finite ensemble of component FI eigenvalue realizations follow a multivariate normal distribution. The characteristics of the realizations therefore are completely determined by the mean vector $\bar{\lambda}$ and covariance matrix Σ or covariance function $\Sigma(x, x')$. In general, the covariance matrix or function corresponding to the FI eigenvalues of a component is unknown. However, a robust assumption [14] that was used in this study is that the covariance function can be defined based on Euclidean distance. Therefore, if $Y(x)$ is a realization of the FI eigenvalues, the covariance function is defined as

$$Cov\big(Y(x), Y(x')\big) = \Sigma(x, x') = exp(-\|x - x'\|^2) \tag{14}$$

where x and x' are two points in FI eigenvalue space. The covariance between $Y(x)$ and $Y(x')$ decays exponentially fast as the distance between x and x' increases. The covariance matrix Σ_n is then generated by evaluating $\Sigma\big(x_i, x_j\big)$ in Eq. (14) at all pairs of the n component FI eigenvalues.

It is apparent that the covariance matrix derived based on Eq. (14) corresponds to unit scale or variance. In practice, it is desired to have the variance of the FI eigenvalues be based on the difference between the FEM and test eigenvalues or frequencies from the component modal test. Suppose that $\Delta\lambda$ is a vector of root-mean-square (RMS) uncertainties assigned to the FI eigenvalues based on the component modal test correlation results. In the case of a Gaussian distribution, the RMS uncertainty is just the standard deviation. The FI eigenvalue covariance matrix with the proper variance is then given by

$$\Sigma_{nv} = diag(\Delta\lambda) * \Sigma_n * diag(\Delta\lambda) \tag{15}$$

where $diag(\Delta\lambda)$ is a diagonal matrix. If the jth eigenvalue λ_j is not uncertain, then $\Delta\lambda_j = 0$ and the jth row and column of Σ_{nv} are null, meaning that Σ_{nv} is positive semi-definite. Within MATLAB®, the command

$$Y = mvnrnd\big(\bar{\lambda}, \Sigma_{nv}, 1\big) \tag{16}$$

produces a finite realization of the random FI eigenvalues under a GP prior with a specific mean and covariance, which can be easily implemented within a MC analysis.

Mixed-Boundary Approach for Assigning HCB Eigenvalue Dispersions

The HPV approach for modeling component uncertainty requires the selection of dispersion values for the HCB component FI eigenvalues, mass matrix, and stiffness matrix. Ideally, these dispersion values are selected for each component based on component modal test results. This is because test-analysis modal correlation metrics are used to determine the dispersions. Test-analysis frequency error is used to identify the HCB FI eigenvalue uncertainties, but one of the biggest challenges in the propagation of component test-analysis frequency error into uncertainty in the HCB flight configuration FI modes is that the component test configuration and the component flight configuration boundary conditions and/or hardware are almost never the same. Because of this, it is difficult to match test configuration modes with flight configuration FI modes. The boundary condition mismatch can be alleviated using a mixed-boundary approach. In general, the HCB flight configuration FI modes

will be over-constrained when compared to the test configuration modes. Therefore, the HCB stiffness matrix in Eq. (1) can be written as

$$K_{HCB} = \begin{bmatrix} K_S & 0 \\ 0 & \lambda \end{bmatrix} = \begin{bmatrix} K_{cc} & K_{cb} & 0 \\ K_{bc} & K_{bb} & 0 \\ 0 & 0 & \lambda \end{bmatrix} \tag{17}$$

where the HCB flight configuration set of boundary degrees of freedom (DOF) have been divided into two subsets: the *c*-set contains all DOF that are free in the component test configuration, and the *b*-set contains the DOF that are constrained in the component test configuration. When the HCB flight configuration is constrained at the test configuration interface DOF (*b*-set), it produces the mass and stiffness matrices

$$M_C = \begin{bmatrix} M_{cc} & M_{cq} \\ M_{qc} & M_{qq} \end{bmatrix} \qquad K_C = \begin{bmatrix} K_{cc} & 0 \\ 0 & \lambda \end{bmatrix} \tag{18}$$

with corresponding eigenvalues λ_C and mass normalized eigenvectors $\phi_C = \begin{bmatrix} \phi_{cc}^T & \phi_{cq}^T \end{bmatrix}^T$. These eigenvalues and eigenvectors are consistent with the boundary conditions of the test configuration modes used in the component test-analysis correlation. Error or uncertainty in the analytical test configuration eigenvalues can be much more easily mapped onto uncertainty $\Delta\lambda_C$ in the eigenvalues of the system in Eq. (18). The HCB representation of the component using λ_C and ϕ_C as FI modal properties has the stiffness matrix and corresponding displacement vector given by

$$K_B = \begin{bmatrix} K_{Sb} & 0 \\ 0 & \lambda_C \end{bmatrix} \qquad u_B = \{x_b^T \quad q_C^T\}^T \tag{19}$$

where K_{Sb} is K_S statically reduced to the *b*-set, x_b is the physical displacement of the *b*-set, and q_C are the modal coordinates of the FI modes with the *c*-set free. The transformation between displacement vector u_B and the original HCB displacement vector u_{HCB} is given by

$$u_{HCB} = \begin{Bmatrix} x_c \\ x_b \\ q \end{Bmatrix} = \begin{bmatrix} \psi & \phi_{cc} \\ I & 0 \\ 0 & \phi_{cq} \end{bmatrix} \begin{Bmatrix} x_b \\ q_C \end{Bmatrix} = T u_B \tag{20}$$

The relation between K_B and K_{HCB} is then

$$K_B = T^T K_{HCB} T \tag{21}$$

The test configuration HCB FI eigenvalues λ_C can be randomized (λ_{Cr}) based upon the component test-analysis correlation results, and the uncertainty can be propagated into the random flight configuration HCB component stiffness (K_{HCBr}) using the expression

$$K_{HCBr} = T^{-T} K_{Br} T^{-1} = T^{-T} \begin{bmatrix} K_{Sb} & 0 \\ 0 & \lambda_{Cr} \end{bmatrix} T^{-1} \tag{22}$$

HURTY/CRAIG-BAMPTON UNCERTAINTY MODELS

The IMT/MSO components used in this UQ analysis were based on the integrated FEM. The FEM was divided into six components and reduced to HCB representations for efficient MC UQ analysis. The frequency range of interest for the IMT is approximately 0.0 to 7.0 Hz., therefore component FI modes were calculated to 15.0 Hz and augmented with residual vectors (RV) corresponding the component interfaces and the IMT shaker locations. A few of the component uncertainty models are described in detail, while the remaining are summarized.

Mass Simulator for Orion

Due to possible scheduling conflicts and the fact that the MPCV would add a multitude of complexities to the IMT, the MPCV was replaced by a mass simulator. The IMT MSO and MSA, shown in Figure 2, were combined into a single FEM

and reduced to an HCB component representation. The HCB component contains 152 DOF including 144 physical DOF at the interface between the MSA and the ICPS, and eight FI modal DOF. Only two of the FI modes have frequencies below 15.0 Hz. The component test/analysis correlation results for the updated MSO are listed in Table 1.

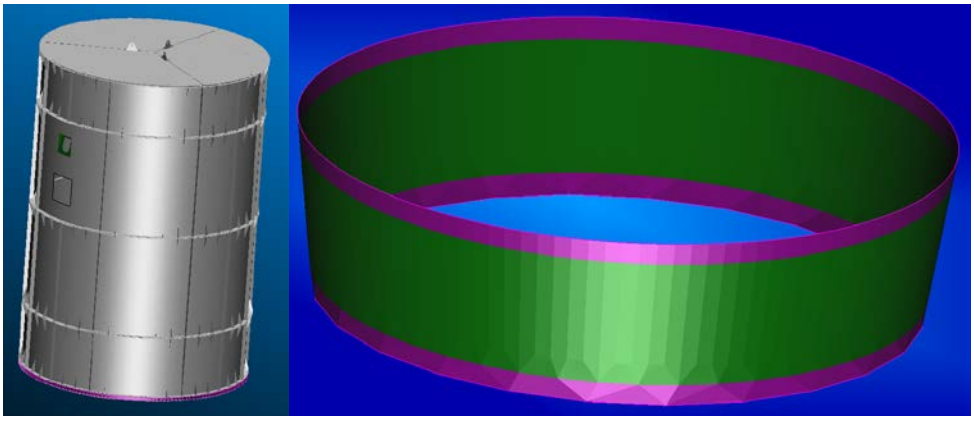

Figure 2: CAD representations of MSO and MSA

Note that the percentage modal frequency errors are computed relative to the FEM frequencies for UQ analysis. There were not enough sensors in the modal test to describe modes 10-14, therefore they were excluded in the formulation of the MSO/MSA uncertainty model. Based on the results in Table 1, the first MSO/MSA HCB FI mode (1st bending along Y) was assigned an RMS uncertainty of 7.97%, and the second MSO/MSA HCB FI mode (1st bending along Z) was assigned an RMS uncertainty of 4.90%. The remaining six FI modes, corresponding to RVs, were assigned an eigenvalue uncertainty of 7.81%, which corresponds to the median eigenvalue uncertainty in MSO FEM test configuration modes 3-9 listed in Table 1. During the process of combining the MSO and MSA FEMs, it was found that the MSO/MSA fixed-base modal frequencies could vary by as much as 10%, depending on just how the interface between the MSO and MSA was modeled. This additional uncertainty was addressed by adding an extra 10% frequency uncertainty, corresponding to approximately 21% eigenvalue uncertainty, to the uncertainties already assigned to the MSO/MSA FI eigenvalues based on the test results. This results in an eigenvalue uncertainty of 28.97% for FI mode one, 25.90% for FI mode two, and 28.81% for the other six FI modes.

Once the eigenvalue uncertainty is applied to the HCB stiffness matrix, the dispersion of the stiffness matrix is then applied using the NPV method. The dispersion level is determined based on the Diagonal Cross-Generalized Mass (DCGM) metric, which is the RMS value of the diagonal of the test/analysis XO matrix. Based on the XO results listed in Table 1, the value of DCGM for the MSO test over the first nine modes is given by $\mathrm{DCGM}_{Test} = 94.84$. An MC analysis was then performed in which the HCB stiffness matrix dispersion was selected and then 3000 random MSO/MSA components were generated. The XO between the nominal and random HCB modes and the corresponding DCGM value were computed for each of the

Table 1: Test/Analysis correlation results for updated MSO

Mode	% Error		XO
	Freq	Eigen	
1	2.42	4.90	99
2	-3.91	-7.97	99
3	3.57	7.27	97
4	4.83	9.89	93
5	3.03	6.15	89
6	5.14	10.55	89
7	3.83	7.81	95
8	1.59	3.20	96
9	5.25	10.78	96
10	3.86	7.88	80
11	4.62	9.44	72
12	6.26	12.92	80
13	5.24	10.76	92
14	3.97	8.09	75

ensemble members for the first nine nominal modes, analogous to the test. The root-sum-square (RSS) cross-orthogonality [15] was computed as the cross-orthogonality for a linear combination of random modes within 3% of the frequency of the unique-best-fit mode. The most probable value of DCGM was then computed over the ensemble and compared with the test value. The stiffness matrix dispersion was adjusted such that the most probable DCGM value for the corresponding ensemble matched the test value. For the MSO/MSA, a stiffness dispersion of $\delta_K = 21\%$ produced a most probable DCGM value of 94.54, which is comparable to the test value. The average RMS frequency uncertainty over the nine HCB modes is 6.72%.

Interim Cryogenic Propulsion Stage

The IMT ICPS and LVSA, shown in Figure 3, were combined and the corresponding FEM was reduced to a single HCB component. The HCB representation contains 306 DOF including 288 physical DOF, 144 at the interface between the MSA and the ICPS, and 144 at the interface between the LVSA and the CS. There are 18 HCB FI modes. The IMT ICPS is empty, so there are no slosh modes. Dispersion values for the updated ICPS/LVSA HCB component were based on the Integrated Spacecraft Payload Element (ISPE) modal test-analysis correlation results. There were 11 FEM target modes matched to 11 of the 19 test modes. Only these target modes were considered in this analysis because the other eight modes were dominated by the MSA/MPCV simulator, which is not part of the ICPS/LVSA component. The test-analysis frequency correlation results are listed in Table 2.

The ISPE was tested in a fixed-base configuration, while the ICPS/LVSA HCB FI modes are constrained at both the base, which is at the interface between the LVSA and the CS, and at the interface between the ICPS and the MSA. This mismatch in boundary conditions makes it difficult to directly match ISPE test configuration modes with the HCB FI modes to assign modal frequency uncertainty. Therefore, the mixed-boundary approach was used on the ICPS/LVSA HCB component. The DOF at the interface between the ICPS and the MSA were released during the component mode calculation, resulting in 162 fixed-base component modes that were compared with the fixed-base modes from the test configuration. However, there are still significant differences between the ICPS/LVSA flight article and the ISPE used in the test. For example, there was no fuel in the test article and the test article included the MSA, a CS simulator and an MPCV simulator. This makes it difficult to use frequency to match ICPS/LVSA fixed-base modes with ISPE test configuration modes. In many cases, test mode descriptions can be used to match modes, but this works best when the modes are low order and the descriptions are relatively simple. In the case of the ISPE, only three of the 11 target modes were easily described and probably insensitive to the hardware differences. Therefore, test-analysis frequency or eigenvalue error was mapped to the ICPS/LVSA fixed-base modes using modal effective mass (MEM). The updated FEM ISPE configuration 3 MEM is dominated by the fundamental bending and, to a lesser extent, the second-order bending modes. The LVSA shell modes have little or no MEM. Table 3 lists

the updated ISPE configuration 3 FEM modes matched to test modes sorted by uncertainty bin based on the MEM Euclidean norm, normalized to a maximum length of $\sqrt{6}$, and multiplied by 100.

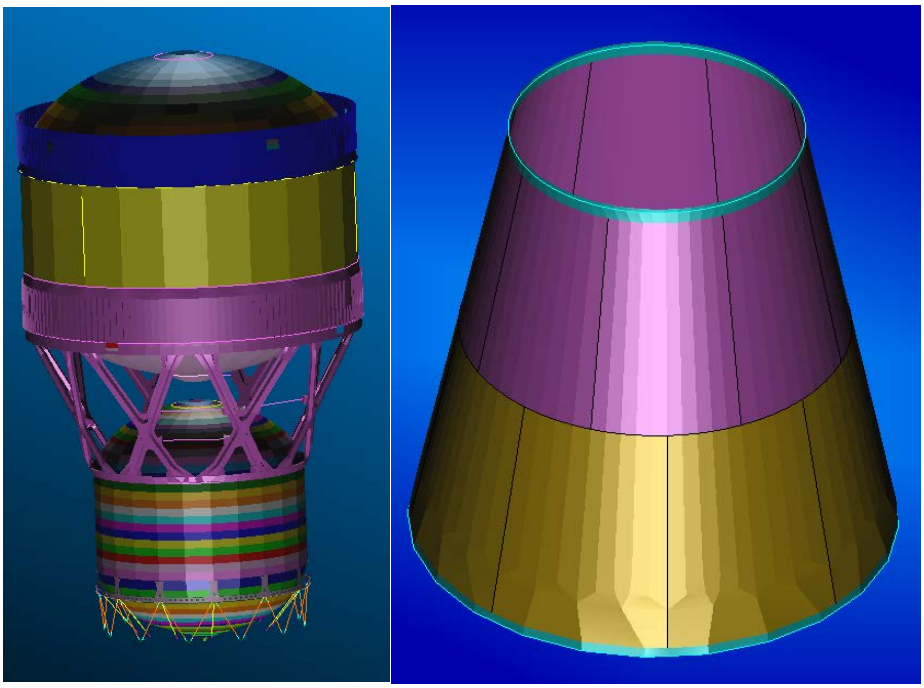

Figure 3: CAD representations of ICPS and LVSA

Table 2: Test-analysis frequency comparison for configuration 3 updated model

FEM Mode	Test Mode	% Error	XO
5	2	-2.70	94
6	1	-0.89	95
7	3	1.43	95
8	4	1.23	95
9	5	3.96	97
10	6	3.50	96
13	10	-0.57	97
14	9	-0.23	97
19	15	-0.33	95
20	14	-0.01	94
24	19	-4.72	94

Bin 1 was assigned a frequency dispersion of 2.02%, corresponding to the RMS error in the prediction of the first bending test mode pair. Bin 2 was assigned a frequency dispersion of 4.72%, corresponding to the test-analysis frequency error of the second-order bending test mode. The remaining LVSA shell test modes have little or no MEM. These modes define uncertainty Bin 3 with a frequency dispersion of 1.95%, corresponding to the RMS frequency error in the LVSA shell modes. MEM was also computed for the ICPS/LVSA fixed-base modes. The first 22 modes to approximately 91 Hz account for approximately 99% of the effective mass over all six rigid body directions. Table 4 lists the first 25 ICPS/LVSA HCB fixed-base modes matched to the test configuration modes sorted by uncertainty bin based on the normalized MEM Euclidean norm. During the UQ analysis the fixed-base mode uncertainty is then mapped into the HCB FI mode uncertainty.

Table 3: ISPE updated FEM MEM magnitude by bin

ISPE FEM Mode	MEM (%)	Bin	% Freq. Dispersion	% Eigen. Dispersion
6	22.30	1	2.02	4.08
5	22.26	1	2.02	4.08
24	2.19	2	4.72	9.66
20	0.02	3	1.95	3.93
19	0.02	3	1.95	3.93
8	0.01	3	1.95	3.93
7	0.00	3	1.95	3.93
9	0.00	3	1.95	3.93
10	0.00	3	1.95	3.93
14	0.00	3	1.95	3.93
13	0.00	3	1.95	3.93

Table 4: IMT ICPS/LVSA HCB fixed-base sorted MEM magnitude and frequency uncertainty by bin

Bin	Number	FB Mode	MEM	% Freq. Dispersion	% Eigen Dispersion
1	1	14	31.91	2.02	4.08
	2	22	27.29	2.02	4.08
	3	18	25.60	2.02	4.08
	4	13	24.52	2.02	4.08
	5	21	14.54	2.02	4.08
	6	15	12.51	2.02	4.08
	7	9	11.34	2.02	4.08
	8	6	10.18	2.02	4.08
2	9	19	6.68	4.72	9.66
	10	20	5.00	4.72	9.66
	11	5	3.98	4.72	9.66
	12	16	3.79	4.72	9.66
	13	10	3.69	4.72	9.66
	14	4	3.66	4.72	9.66
	15	3	1.21	4.72	9.66
	16	2	1.21	4.72	9.66
	17	7	1.13	4.72	9.66
	18	17	0.97	4.72	9.66
3	19	23	0.61	1.95	3.93
	20	25	0.51	1.95	3.93
	21	8	0.29	1.95	3.93
	22	1	0.17	1.95	3.93
	23	11	0.16	1.95	3.93
	24	24	0.05	1.95	3.93
	25	12	0.03	1.95	3.93

Based on the XO results listed in Table 2, the value of DCGM for the ISPE configuration 3 test over the 11 FEM/test mode pairs is given by $\mathrm{DCGM}_{Test} = 95.44$. An MC analysis was performed in which the stiffness matrix dispersion was selected

and then 3000 random ICPS/LVSA components were generated. The 3% RSS XO between the nominal and random HCB modes and the corresponding DCGM value were computed for each of the ensemble members for the first 19 nominal modes below 15 Hz. A stiffness dispersion of $\delta_K = 15\%$ produced a most probable DCGM value of 95.74, which is comparable to the test value. The average RMS frequency uncertainty over the 19 HCB modes is 2.78%.

Core Stage

The IMT CS FEM, shown in Figure 4, was reduced to an HCB component with 224 DOF, including 168 physical DOF, 144 at the interface between the LVSA and the CS, and another 24 DOF at the interfaces between the CS and the SRBs. There are 56 HCB FI modes. The IMT CS is empty, so there are no slosh modes, but CS pressurization stiffness is included. The IMT CS test-analysis correlation results are shown in Table 5. Eight test configuration IMT CS modes were matched with eight

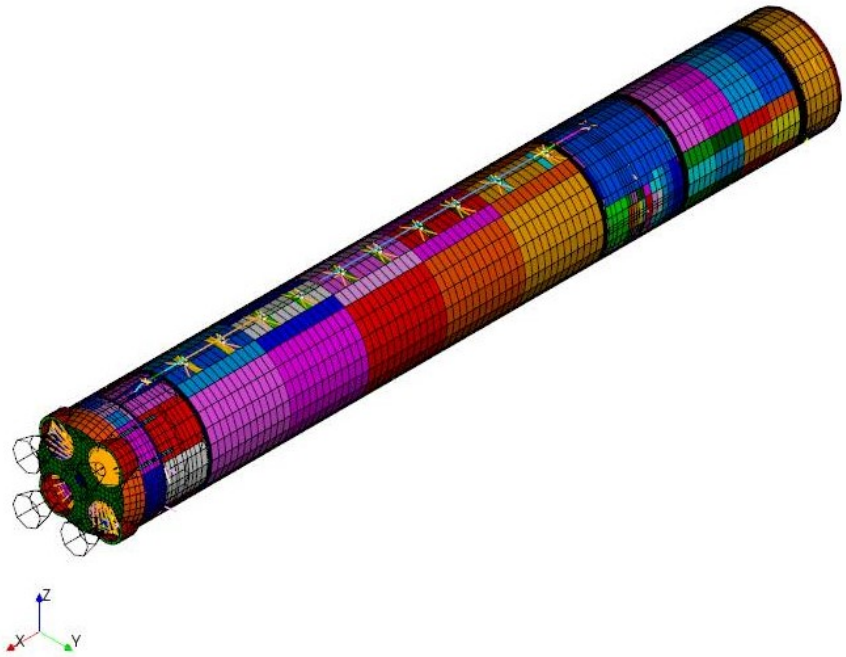

Figure 4: CS finite element model

test modes. The CS was tested in a simulated free-free configuration, therefore, as in the case of the ICPS/LVSA, there is a mismatch between the test configuration boundary conditions and the boundary conditions applied to the CS HCB FI modes. Therefore, the mixed-boundary approach was also applied to the IMT CS. In order to match the test configuration boundary conditions, all 168 HCB interface DOF were released, resulting in 224 free-free CS HCB modes that were compared with the CS test configuration modes. The eigenvalue dispersions of the HCB component modes were based on the test-analysis correlation results listed in Table 5. However, matching modes between the two sets to determine uncertainty could not be performed using MEM, as in the case of the ICPS/LVSA, because the modes are unconstrained, so they possess no MEM. Instead, the free-free CS HCB component modes were matched to the eight test configuration modes purely by the mode description listed in Table 5. The corresponding test-analysis eigenvalue error was then assigned to the HCB free-free component mode as the RMS eigenvalue uncertainty. The resulting eigenvalue uncertainties for the IMT CS HCB free-free component modes are listed in Table 6. Note that there are 18 HCB modes matched to the eight test configuration modes because there are 8 HCB engine pendulum modes and the HCB bending modes are not purely bending and instead are more complex bending mode pairs. In addition, to be conservative, all HCB modes matched to the 2nd bending mode about Z test configuration mode were given an eigenvalue uncertainty that is equal to the 8.65% uncertainty corresponding to the 2nd bending about Y test configuration mode instead of the 0% uncertainty listed in Table 5. The remaining 188 elastic HCB free-free modes were assigned an eigenvalue dispersion of 6.27%, which corresponds to median eigenvalue uncertainty in the 8 test configuration modes listed in Table 4. The median was used instead of the mean such that no one mode would have too much influence.

Table 5: IMT CS modal test-analysis correlation results

Test Mode	% Error		XOR
	Freq	Eigen	
1	-2.90	5.88	99
2	-6.90	14.27	98
3	10.71	22.58	43
4	3.27	6.66	79
5	4.23	8.65	87
6	0	0	89
7	-0.44	0.89	95
8	-0.29	0.59	89

Based on the XO results listed in Table 4, the value of DCGM for the CS test over the 7 FEM/test mode pairs, excluding the engine pendulum mode pair, is given by $\mathrm{DCGM}_{Test} = 91.09$. The XO value for the engine pendulum mode was excluded because it was uncommonly low, and not reflective of the overall quality of the test. MC analysis using 3000 ensemble members and 3% RSS XO was performed to determine the HCB stiffness matrix dispersion. The DCGM metric for each ensemble member was calculated over the first 48 elastic modes. For the CS HCB, a stiffness dispersion of $\delta_K = 8.5\%$ produced a most probable DCGM value of 91.03, which approximates the test value. The average RMS frequency uncertainty over the 48 HCB modes is 4.70%.

Table 6: IMT CS HCB free-free mode eigenvalue dispersions

	% Dispersion	
Mode	Freq	Eigen
23	2.90	5.88
24	6.90	14.27
25	2.90	5.88
26	10.72	22.58
28	10.72	22.58
31	10.72	22.58
32	10.72	22.58
36	3.28	6.66
45	10.72	22.58
46	10.72	22.58
47	10.72	22.58
48	10.72	22.58
57	0.44	0.89
67	0.29	0.59
72	4.24	8.65
73	4.24	8.65
78	4.24	8.65
79	4.24	8.65

Uncertainty models were also generated for the SRBs and the ML using the approaches outlined in the previous subsections. There was no specific modal test performed for the SLS SRBs, however due to the SRB's heritage, the uncertainty models for the IMT SRB HCB components were assumed to be at the updated level. It was also assumed that the SRBs have approximately the same level of test-analysis correlation, or uncertainty, as found in the updated ISPE, listed in Table 3. This means that the three HCB FI eigenvalue uncertainty bins are given by 4.08%, 9.66% and 3.93%, and the HCB stiffness

dispersion of 2.5% was adjusted to produce a most probable DCGM value of 95.44 corresponding to the updated ISPE DCGM test value. The RSRB HCB component was assigned the same uncertainty model as the LSRB.

The IMT ML FEM was constrained at the six VAB support posts and reduced to an HCB representation with 401 DOF, including 24 DOF that interface with other components, 366 FI modes to 15.0 Hz. and 11 RVs. A modal survey of the ML only on the VAB support posts was performed at Kennedy Space Center on June 16-26, 2019. Test-analysis correlation results for the IMT ML are shown in Table 7 for 15 target modes, 14 primary and one secondary. Note that target mode three is a Crew Access Arm (CAA) mode that was in a different orientation during the modal test than what was modeled in the ML, therefore producing the large frequency error listed. For that reason, ML mode three was eliminated from the target mode set during the derivation of the IMT ML uncertainty model.

There is a mismatch between the ML test configuration boundary conditions and those applied to the ML HCB FI modes. Therefore, the mixed-boundary approach was also applied to the ML HCB to assign eigenvalue dispersions. The 24 HCB interface DOF were released during HCB mode computation, resulting in 401 fixed-base modes. The HCB fixed-base modes were directly matched to the test configuration target modes listed in Table 7 using MEM and mode descriptions. The corresponding test configuration eigenvalue errors were assigned as dispersions to the corresponding HCB fixed-base modes. The remaining HCB fixed-base modes were assigned an eigenvalue dispersion of 3.35%, corresponding to the median eigenvalue error for the 14 target modes remaining after mode three was removed. Based on the XO values in Table 7, the test value of the DCGM metric over the 14 target modes is 89.77. During the MC stiffness dispersion analysis, the DCGM metric was computed for each ensemble member for the first 44 elastic modes with frequencies less than 8.0 Hz. An HCB stiffness dispersion of 4% produced a most probable DCGM value of 90.58, which was comparable to the test value. The corresponding mean RMS frequency uncertainty was 2.25% over the 44 modes

Table 7: Test-analysis correlation results for IMT ML on VAB support posts

Test	FEM	% Error		
Mode	Mode	Freq	Eigen	XO
1	1	0.30	0.60	98
2	2	1.97	3.97	100
3	3	-23.36	-52.19	95
4	4	3.30	6.72	98
5	5	0.49	0.99	92
6	6	-2.57	-5.21	94
7	7	-3.17	-6.43	95
8	8	-0.43	-0.87	95
9	9	1.24	2.50	86
10	10	3.59	7.32	98
11	11	-2.56	-5.20	93
12	12	-0.81	-1.64	82
13	13	-1.36	-2.74	88
14	14	3.39	6.89	70
16	21	-0.77	-1.55	57

IMT UQ ANALYSIS

A UQ analysis was performed for the IMT configuration using MC analysis with an ensemble of 10,105 random models. The goals of the analysis were to determine the amount of primary target mode frequency and shape uncertainty that could be expected during the actual IMT, and the corresponding probability that the selected shaker and sensor configurations will adequately excite and separate the primary target modes. This work was completed prior to the IMT, however during future post-test analysis, it is expected that the test results will be compared to the UQ predictions. If the uncertainty predicted by

the UQ analysis covers the test results, there will be increased confidence in the HPV UQ method and the approach used to assign component uncertainty models.

The reduced IMT model contains 941 DOF and there are 70 modes below approximately 7 Hz. Twenty-two primary target modes were considered in this assessment. Table 8 lists the primary target modes with partial mode descriptions. The component uncertainty models described previously are summarized in Table 9.

Table 8: IMT primary target modes

No.	Mode	Description
1	1	SLS Rocking XZ Plane
2	2	ML Tower 1st Bending XZ Plane
3	3	SLS 1st XY Bending
4	4	ML Tower 1st Bending XY Plane
5	6	Core 1st Torsion
6	7	SLS 1st XZ Bending
7	8	SLS 2nd XZ Bending
8	9	SLS 2nd XY Bending
9	10	SRB 1st Bending
10	11	SLS 3rd XY Bending
11	12	ML Tower Torsion
12	13	ML Tower 2nd XZ Bending
13	14	ML Tower/SLS 2nd XY Bending
14	15	ML Trampoline
15	16	CAA Vertical/SLS Bending
16	17	CAA Vertical/SLS Bending
17	18	CAA Vertical
18	19	ML Twisting/Tower Torsion
19	21	SLS 2nd Torsion
20	22	ML Tower Bounce/3rd Bending
21	23	ML Tower 3rd XZ Bending
22	27	SRB 2nd XY Bending/CAA lateral

Table 9: IMT uncertainty model

Component	Uncertainty Level	Assigned HCB FI Frequency Dispersion %	Stiffness Dispersion %	Normalized Stiffness Dispersion %
MSO	Updated	Modes: 3.91, 2.42; RVs: 3.83	21	3.11
ICPS/LVSA	Updated	3-Bins: 2.02, 4.72, 1.95	15	1.78
CS	Updated	Table 6	8.5	0.88
LSRB	Updated	3-Bins: 2.02, 4.72, 1.95	2.5	0.75
RSRB	Updated	3-Bins: 2.02, 4.72, 1.95	2.5	0.75
ML	Updated	Table 7	4	1.16

Based on the UQ analysis, the RMS uncertainty for the 22 target modes is illustrated in Figure 5. The greatest uncertainty, 3.23%, is in mode 19, which corresponds to the ML twisting/tower torsion mode. Figure 6 presents error bars for the target mode frequencies representing the range between the upper tolerance level at P99/90 and the lower tolerance level at P01/90. The corresponding interval provides an estimate of 98% enclosure with 90% confidence (P98/90). It can be seen that all of the modes possess a relatively small amount of frequency uncertainty. The nominal and median target mode frequencies are close in all 22 target modes. Figure 7 shows the corresponding primary target mode RMS XO. Twenty of the target modes possess an RMS XO value greater than 0.90, while two have values between 0.80 and 0.90. Note that no RSS analysis was performed to compute the XO values in this case.

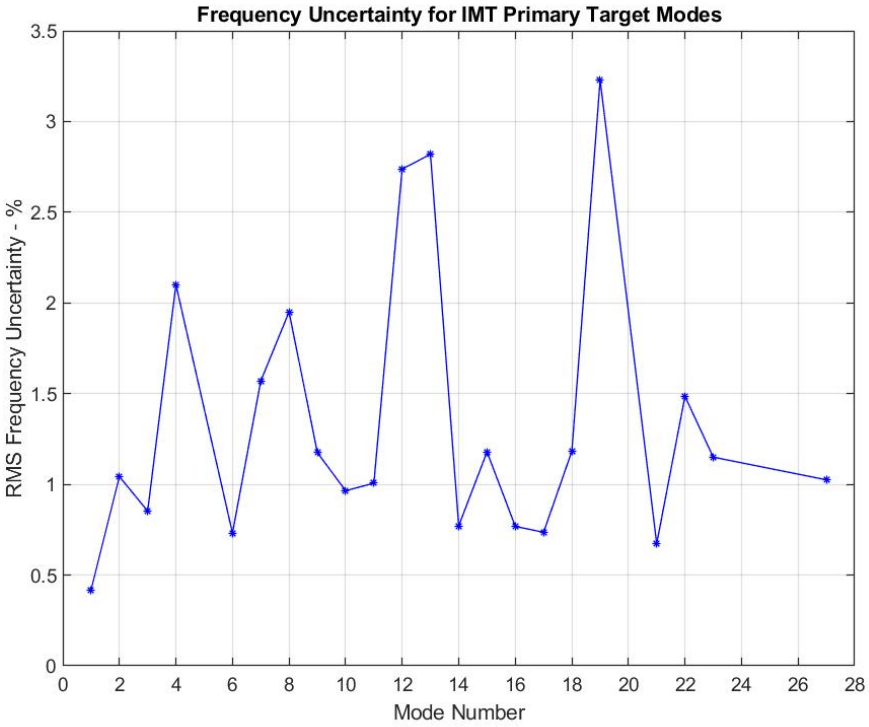

Figure 5**:** RMS frequency uncertainty for IMT primary target modes

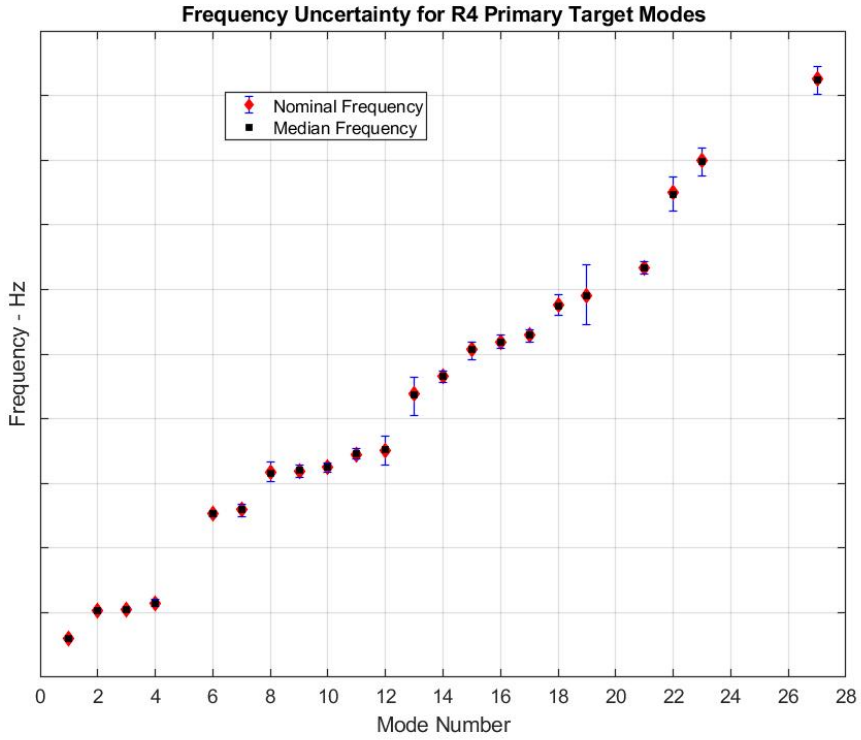

Figure 6: P98/90 coverage intervals for IMT primary target mode frequencies

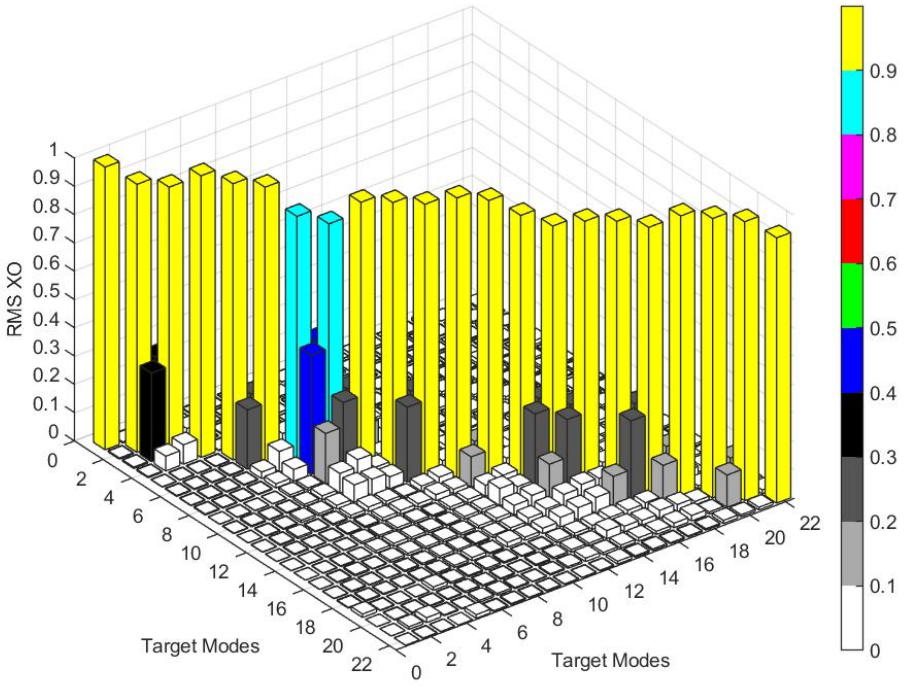

Figure 7**:** IMT primary target mode RMS cross-orthogonality

The IMT sensor set contains 195 accelerometers. Figure 8 shows the XO between the nominal primary target modes and the nominal IMT modes below approximately 6 Hz with unobservable modes 20, 24, and 32 removed. The XO was computed using the IMT test analysis model (TAM) with the modes mass normalized with respect to the TAM mass. The largest off-diagonal value of 0.058 indicates that the target modes are nicely decoupled from the other observable IMT modes using the IMT sensor configuration and TAM mass matrix.

During each iteration of the MC analysis, the random system modes were uniquely matched to the nominal system modes. The random modes were then recovered at the sensor DOF and mass normalized with respect to the nominal TAM mass matrix. The XO between the random target modes and the random observable modes using the TAM mass matrix was computed and the largest off-diagonal magnitude for each target mode was saved. Figure 9 shows the nominal, median, and the P98/90 enclosure intervals for the maximum off-diagonal values for each of the target modes. All nominal values are below 0.04. For the most part, the median values are close to the nominal values. The P99/90 maximum off-diagonal values are less than 0.06 for all the target modes, except target mode 27, which is the SRB 2nd bending/CAA lateral bending mode. Figure 9 shows that the P99/90 value for mode 27 is much larger than both the nominal and median values, indicating that there is a large tail in the distribution of the maximum off-diagonal values. Even though the P99/90 maximum off-diagonal value is greater than 0.25, it can be shown that there is over a 92% probability that the maximum off-diagonal value is less than or equal to 0.10, which is often cited as the orthogonality criterion. These results indicate that during the actual IMT, there is high probability and confidence that the first 21 target modes can be separated from the observable modes below approximately 6 Hz. In addition, there is a significant probability that target mode 27 can also be separated.

Statistics were also computed for acceleration frequency response and normal mode indicator functions for the selected shaker and sensor configurations. A modal damping level of 1.0% and modes up to 16.0 Hz. were included in the simulations. The shaker configuration selected for this assessment is listed in Table 10. A typical acceleration frequency response in the Y direction on the ICPS/LVSA due to input at shaker S36 along X is shown in Figure 10. The nominal as well as the P99/90 and P01/90 response levels are illustrated. During IMT post-test analysis, the corresponding test result can

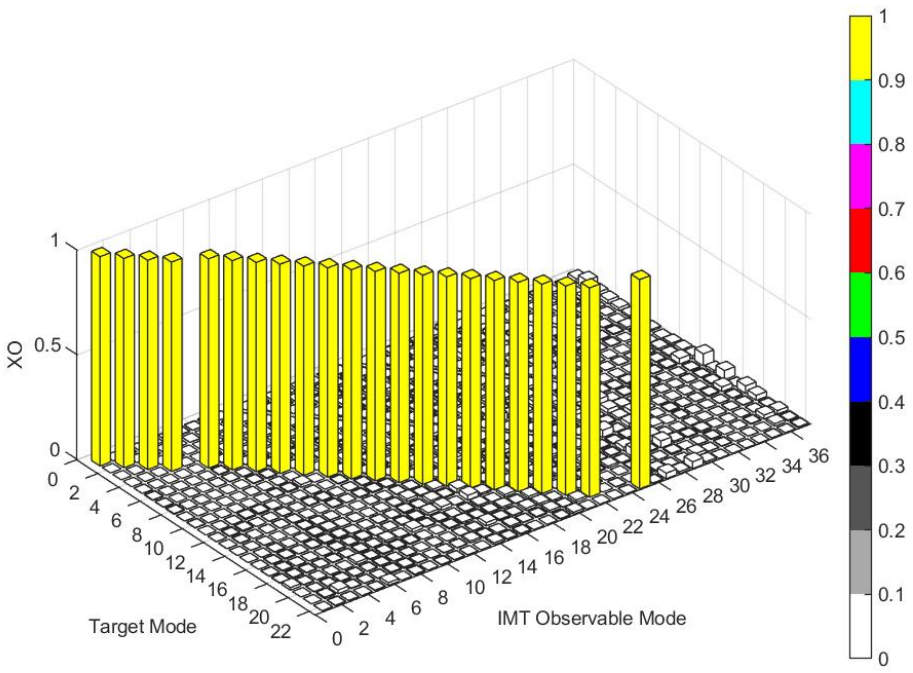

Figure 8**:** XO between target modes and all observable IMT modes below 5.46 Hz

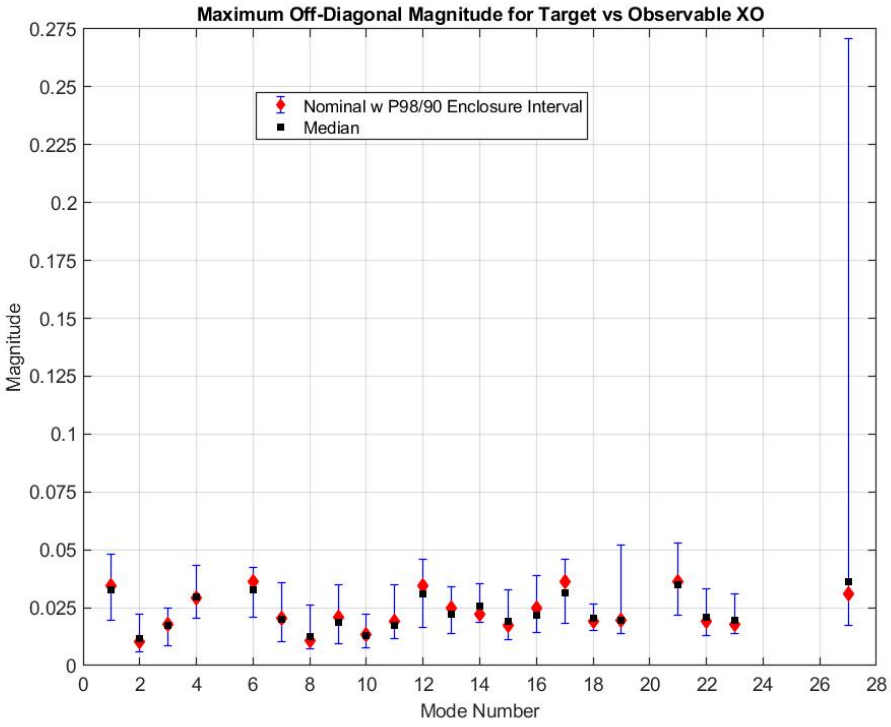

Figure 9**:** Maximum off-diagonal statistics for XO between target and all observable IMT modes below 6 Hz

be compared with the predicted uncertainty interval shown in the figure. If the test result lies within the uncertainty interval, confidence in the validity of the HPV UQ method is enhanced.

Table 10: IMT shaker configuration

	Shaker Label	Dir.
1	S32	X
2	S35	X
3	S36	X
4	S38	Y
5	S40	Z
6	S50	X
7	S51	Y

The NMIF can be used to determine how effectively each of the primary target modes is excited and measured using the proposed shaker/sensor configuration. In practice, an NMIF value of 0.3 or smaller indicates that the mode is sufficiently excited and measured to be extracted from the test frequency response data. Therefore, for a mode to be sufficiently excited and measured, it must have an NMIF value less than or equal to 0.30 for any of the shakers. Figure 11 illustrates the minimum NMIF value over all of the shakers for each of the primary target modes for the nominal system. The values were determined by evaluating the NMIF functions at the nominal target mode frequencies. This approach is conservative because the minimum of the NMIF does not in general occur at the resonance, so this approach does not always capture the true minimum value. Using the criterion of NMIF being less than or equal to 0.30, 20 of the 22 primary IMT target modes

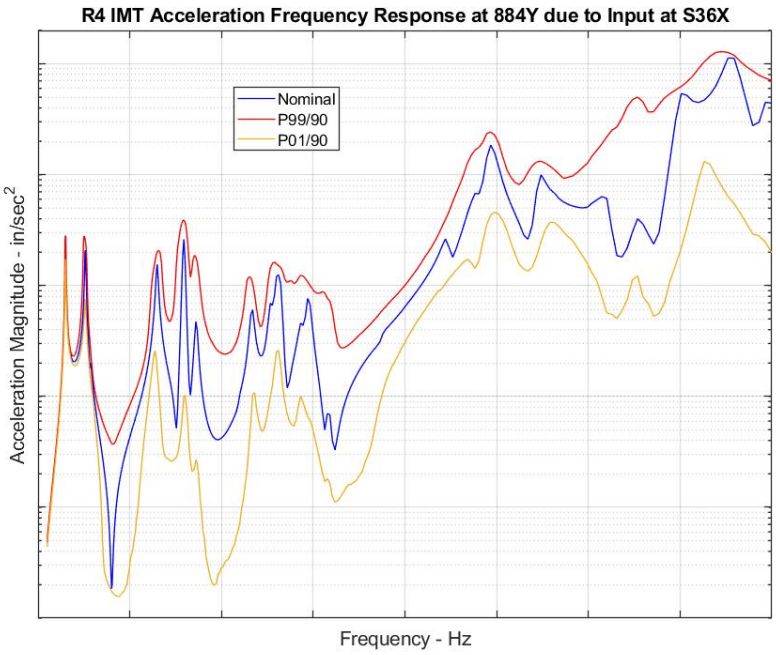

Figure 10**:** Acceleration frequency response on ICPS along Y due to input from shaker S36X

are sufficiently excited and measured using the proposed IMT shaker/sensor configuration. Figure 11 also shows the minimum P99/90 and P01/90 NMIF values for each target mode over all seven shakers. The NMIF values corresponding to the random systems are determined by uniquely matching each of the nominal system target modes to a random mode and then evaluating the random NMIF function at the corresponding random resonant frequency. It can be seen from the figure, that there is a significant amount of uncertainty in the NMIF values for all of the target modes except the first. The median values of the target mode NMIF values over the ensemble are also presented in Figure 10. In many cases, the median NMIF values are close to the nominal values. Applying the 0.30 criterion to the median NMIF values, the figure indicates that there is a 50% probability of identifying all of the target modes during the IMT. Seven of the target modes have P99/90 NMIF values less than 0.30.

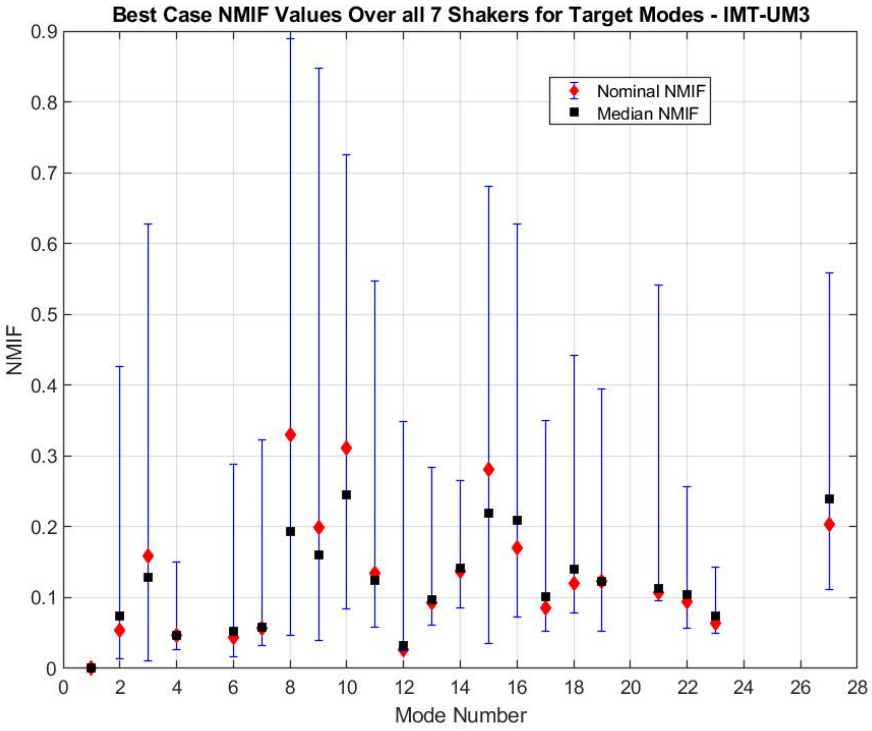

Figure 11**:** IMT primary target mode NMIF statistics for 7 shakers

CONCLUSION

NASA has historically tested launch vehicles in an integrated configuration with boundary conditions controlled to approximate the boundary conditions expected in flight. However, to save cost and schedule, a cross-program decision was made to not perform an IVGVT and rely on analytical methods supported by component test results. However, there will still be an integrated system that will undergo testing, called the Integrated Modal Test. The IMT is a ground test of the integrated vehicle, assembled on the ML in VAB facility at Kennedy Space Center. The results of the IMT will provide an opportunity to validate or update previously correlated SLS component models such that, in an assembled configuration, they provide agreement with integrated system test results. The purpose of this assessment was to apply the HPV UQ approach to the IMT/MSO ground vibration test configuration. Projection of component test-based uncertainty into the system provided estimates of the system-level uncertainty that can be expected in IMT target modal parameters, such as frequencies and mode shapes. Component uncertainty was also propagated into system level acceleration frequency response and corresponding mode indicator functions. The HPV method combines a parametric variation of the HCB FI modal frequencies with an NPV method that randomly varies the HCB stiffness matrices as Wishart random matrix distributions using RMT. Uncertainty models were developed for each of the HCB components using the test-analysis correlation results from component test-configuration modal tests. The component uncertainty was propagated to the system level using a MC approach that generated statistics for system-level results. This provided a UQ method that can be traced directly to available test data, and which can be updated as additional data and better correlated models become available. In order to be more consistent with future IMT test and analysis, the most recent IMT configuration model was used in the UQ analysis. The finite element model was divided into six elements and reduced to the corresponding HCB components. Model correlation and updating of the ML is still in progress, meaning that the sensor set and shaker locations are still evolving. It has been found that the ability of the shaker configuration to adequately excite the target modes is very dependent on the most recent updated ML model version.

During the MC analysis, the off-diagonal elements in the XO between the random target modes and the random observable modes using the TAM mass matrix was computed and the largest off-diagonal magnitude for each target mode tracked. All nominal system maximum off-diagonal values were below 0.05 except target mode 14. The P99/90 maximum off-diagonal

values were less than 0.10 for all the target modes, except target mode 27, which is the SRB 2nd bending/CAA lateral bending mode. Even though the P99/90 maximum off-diagonal value for mode 27 was greater than 0.25, there was still over a 92% probability that its value would be less than or equal to 0.10, which is often cited as the orthogonality criterion. These results indicate that during the actual IMT, there is high probability and confidence that the first 21 target modes can be separated from the observable modes below approximately 6 Hz. In addition, there is a significant probability that target mode 27 can be separated. Using the criterion that the NMIF must be less than or equal to 0.30, 20 of the 22 primary IMT target modes are sufficiently excited and measured using the proposed IMT seven-shaker/sensor configuration. Applying the 0.30 criterion to the median NMIF values, there is a 50% probability of identifying all of the target modes during the IMT. Seven of the target modes have P99/90 NMIF values less than 0.30. While the results of this UQ assessment provide meaningful insight into the effects of component uncertainty on system level results, the assessment was not meant to be a comprehensive UQ analysis of the SLS IMT. For simplicity, noteworthy sources of uncertainty, such as component damping, were neglected in this assessment. In future work, it is believed that the HPV approach can also be applied to the dispersion of the component damping matrix. Finally, while the HPV method provides a valuable tool for complex system UQ analysis using only a limited amount of data, it is believed that confidence in predicted results could be improved through a rigorous validation program.

REFERENCES

[1] R. R. Craig and M. C. C. Bampton, "Coupling of Substructures for Dynamic Analysis," *AIAA Journal*, vol. 6, pp. 1313-1319, 1968.

[2] D. Kammer, P. Blelloch and J. Sills, "Test-Based Uncertainty Quantification and Propagation Using Hurty/Craig-Bampton Substructure Representations," in *IMAC*, Orlando, FL, 2019.

[3] Kammer, D.; Blelloch, P.; and Sills, J.: “Variational Coupled Loads Analysis using the Hybrid Parametric Variation Method,” in *IMAC*, Houston, TX, 2020.

[4] J. Wishart, "Generalized product moment distribution in samples," *Biometrika*, vol. 20A), no. 1-2, pp. 32-52, 1928.

[5] Rades, M.: “Performance of Various Mode Indicator Functions,” *Shock and Vibration*, vol. 17, 473–482, 2010.

[6] R. Ghanem and P. Spanos, Stochastic Finite Elements: A Spectral Approach, New York: Springer, 1991.

[7] C. Soize, "A Nonparametric Model of Random Uncertainties for Reduced Matrix Models in Structural Dynamics," *Probabilistic Engineering Mechanics*, vol. 15, no. 3, pp. 277-294, 2000.

[8] C. Soize, "Maximum Entropy Approach for Modeling Random Uncertainties in Transient Elastodynamics," *J. Acoust. Soc. Am.*, vol. 109, no. 5, pp. 1979-1996, 2001.

[9] S. Adhikari, "Generalized Wishart Distribution for Probabilistic Structural Dynamics," *Comput. Mech.*, vol. 45, pp. 495-511, 2010.

[10] S. Adhikari, "Wishart Random Matrices in Probabilistic Structural Mechanics," *J. Eng. Mech.*, vol. 134, no. 12, pp. 1029-1044, 2008.

[11] E. Capiez-Lernout, M. Pellissetti, H. Pradlwarter, G. I. Schueller and C. Soize, "Data and model uncertainties in complex aerospace engineering systems," *J. Sound Vib.*, vol. 295, no. 3-5, p. 923–938, 2006.

[12] M. Pellissetti, E. Capiez-Lernout, r. H. Pradlwarte, C. Soize and G. Schueller, "Reliability analysis of a satellite structure with a parametric and a non-parametric probabilistic model," *Comput. Methods Appl. Mech. Eng.*, vol. 198, no. 2, p. 344–357., 2008.

[13] M. Mignolet, S. C and J. Avalos, "Nonparametric Stochastic Modeling of Structures with Uncertain Boundary Conditions / Coupling Between Substructures," *AIAA J.*, vol. 51, no. 6, p. 1296–1308, 2013.

[14] Gramacy, R.: *Surrogates, Gaussian Process Modeling, Design, and Optimization for the Applied Sciences*, CRC Press, Boca Raton, FL, 2020.

[15] Blelloch, P.: “Cross-Orthogonality of Closely Spaced Modes,” in *IMAC*, 2006.